FERMILAB-PUB-13-011-E

Measurement of the ratio of differential cross sections $\sigma(p\bar{p} \to Z + b \text{ jet})/\sigma(p\bar{p} \to Z + \text{jet})$ in $p\bar{p}$ collisions at $\sqrt{s} = 1.96$ TeV

V.M. Abazov,[32] B. Abbott,[68] B.S. Acharya,[26] M. Adams,[46] T. Adams,[44] G.D. Alexeev,[32] G. Alkhazov,[36] A. Alton[a],[57] A. Askew,[44] S. Atkins,[55] K. Augsten,[7] C. Avila,[5] F. Badaud,[10] L. Bagby,[45] B. Baldin,[45] D.V. Bandurin,[44] S. Banerjee,[26] E. Barberis,[56] P. Baringer,[53] J.F. Bartlett,[45] U. Bassler,[15] V. Bazterra,[46] A. Bean,[53] M. Begalli,[2] L. Bellantoni,[45] S.B. Beri,[24] G. Bernardi,[14] R. Bernhard,[19] I. Bertram,[39] M. Besançon,[15] R. Beuselinck,[40] P.C. Bhat,[45] S. Bhatia,[59] V. Bhatnagar,[24] G. Blazey,[47] S. Blessing,[44] K. Bloom,[60] A. Boehnlein,[45] D. Boline,[65] E.E. Boos,[34] G. Borissov,[39] A. Brandt,[71] O. Brandt,[20] R. Brock,[58] A. Bross,[45] D. Brown,[14] J. Brown,[14] X.B. Bu,[45] M. Buehler,[45] V. Buescher,[21] V. Bunichev,[34] S. Burdin[b],[39] C.P. Buszello,[38] E. Camacho-Pérez,[29] B.C.K. Casey,[45] H. Castilla-Valdez,[29] S. Caughron,[58] S. Chakrabarti,[65] D. Chakraborty,[47] K.M. Chan,[51] A. Chandra,[73] E. Chapon,[15] G. Chen,[53] S.W. Cho,[28] S. Choi,[28] B. Choudhary,[25] S. Cihangir,[45] D. Claes,[60] J. Clutter,[53] M. Cooke,[45] W.E. Cooper,[45] M. Corcoran,[73] F. Couderc,[15] M.-C. Cousinou,[12] D. Cutts,[70] A. Das,[42] G. Davies,[40] S.J. de Jong,[30,31] E. De La Cruz-Burelo,[29] F. Déliot,[15] R. Demina,[64] D. Denisov,[45] S.P. Denisov,[35] S. Desai,[45] C. Deterre[d],[20] K. DeVaughan,[60] H.T. Diehl,[45] M. Diesburg,[45] P.F. Ding,[41] A. Dominguez,[60] A. Dubey,[25] L.V. Dudko,[34] D. Duggan,[61] A. Duperrin,[12] S. Dutt,[24] A. Dyshkant,[47] M. Eads,[47] D. Edmunds,[58] J. Ellison,[43] V.D. Elvira,[45] Y. Enari,[14] H. Evans,[49] V.N. Evdokimov,[35] G. Facini,[56] L. Feng,[47] T. Ferbel,[64] F. Fiedler,[21] F. Filthaut,[30,31] W. Fisher,[58] H.E. Fisk,[45] M. Fortner,[47] H. Fox,[39] S. Fuess,[45] A. Garcia-Bellido,[64] J.A. García-González,[29] G.A. García-Guerra[c],[29] V. Gavrilov,[33] W. Geng,[12,58] C.E. Gerber,[46] Y. Gershtein,[61] G. Ginther,[45,64] G. Golovanov,[32] P.D. Grannis,[65] S. Greder,[16] H. Greenlee,[45] G. Grenier,[17] Ph. Gris,[10] J.-F. Grivaz,[13] A. Grohsjean[d],[15] S. Grünendahl,[45] M.W. Grünewald,[27] T. Guillemin,[13] G. Gutierrez,[45] P. Gutierrez,[68] J. Haley,[56] L. Han,[4] K. Harder,[41] A. Harel,[64] J.M. Hauptman,[52] J. Hays,[40] T. Head,[41] T. Hebbeker,[18] D. Hedin,[47] H. Hegab,[69] A.P. Heinson,[43] U. Heintz,[70] C. Hensel,[20] I. Heredia-De La Cruz,[29] K. Herner,[57] G. Hesketh[f],[41] M.D. Hildreth,[51] R. Hirosky,[74] T. Hoang,[44] J.D. Hobbs,[65] B. Hoeneisen,[9] J. Hogan,[73] M. Hohlfeld,[21] I. Howley,[71] Z. Hubacek,[7,15] V. Hynek,[7] I. Iashvili,[63] Y. Ilchenko,[72] R. Illingworth,[45] A.S. Ito,[45] S. Jabeen,[70] M. Jaffré,[13] A. Jayasinghe,[68] M.S. Jeong,[28] R. Jesik,[40] P. Jiang,[4] K. Johns,[42] E. Johnson,[58] M. Johnson,[45] A. Jonckheere,[45] P. Jonsson,[40] J. Joshi,[43] A.W. Jung,[45] A. Juste,[37] E. Kajfasz,[12] D. Karmanov,[34] P.A. Kasper,[45] I. Katsanos,[60] R. Kehoe,[72] S. Kermiche,[12] N. Khalatyan,[45] A. Khanov,[69] A. Kharchilava,[63] Y.N. Kharzheev,[32] I. Kiselevich,[33] J.M. Kohli,[24] A.V. Kozelov,[35] J. Kraus,[59] A. Kumar,[63] A. Kupco,[8] T. Kurča,[17] V.A. Kuzmin,[34] S. Lammers,[49] G. Landsberg,[70] P. Lebrun,[17] H.S. Lee,[28] S.W. Lee,[52] W.M. Lee,[44] X. Lei,[42] J. Lellouch,[14] D. Li,[14] H. Li,[74] L. Li,[43] Q.Z. Li,[45] J.K. Lim,[28] D. Lincoln,[45] J. Linnemann,[58] V.V. Lipaev,[35] R. Lipton,[45] H. Liu,[72] Y. Liu,[4] A. Lobodenko,[36] M. Lokajicek,[8] R. Lopes de Sa,[65] R. Luna-Garcia[g],[29] A.L. Lyon,[45] A.K.A. Maciel,[1] R. Magaña-Villalba,[29] S. Malik,[60] V.L. Malyshev,[32] Y. Maravin,[54] J. Martínez-Ortega,[29] R. McCarthy,[65] C.L. McGivern,[41] M.M. Meijer,[30,31] A. Melnitchouk,[45] D. Menezes,[47] P.G. Mercadante,[3] M. Merkin,[34] A. Meyer,[18] J. Meyer,[20] F. Miconi,[16] N.K. Mondal,[26] M. Mulhearn,[74] E. Nagy,[12] M. Naimuddin,[25] M. Narain,[70] R. Nayyar,[42] H.A. Neal,[57] J.P. Negret,[5] P. Neustroev,[36] H.T. Nguyen,[74] T. Nunnemann,[22] J. Orduna,[73] N. Osman,[12] J. Osta,[51] M. Padilla,[43] A. Pal,[71] N. Parashar,[50] V. Parihar,[70] S.K. Park,[28] R. Partridge[e],[70] N. Parua,[49] A. Patwa,[66] B. Penning,[45] M. Perfilov,[34] Y. Peters,[20] K. Petridis,[41] G. Petrillo,[64] P. Pétroff,[13] M.-A. Pleier,[66] P.L.M. Podesta-Lerma[h],[29] V.M. Podstavkov,[45] A.V. Popov,[35] M. Prewitt,[73] D. Price,[49] N. Prokopenko,[35] J. Qian,[57] A. Quadt,[20] B. Quinn,[59] M.S. Rangel,[1] K. Ranjan,[25] P.N. Ratoff,[39] I. Razumov,[35] P. Renkel,[72] I. Ripp-Baudot,[16] F. Rizatdinova,[69] M. Rominsky,[45] A. Ross,[39] C. Royon,[15] P. Rubinov,[45] R. Ruchti,[51] G. Sajot,[11] P. Salcido,[47] A. Sánchez-Hernández,[29] M.P. Sanders,[22] A.S. Santos[i],[1] G. Savage,[45] L. Sawyer,[55] T. Scanlon,[40] R.D. Schamberger,[65] Y. Scheglov,[36] H. Schellman,[48] C. Schwanenberger,[41] R. Schwienhorst,[58] J. Sekaric,[53] H. Severini,[68] E. Shabalina,[20] V. Shary,[15] S. Shaw,[58] A.A. Shchukin,[35] R.K. Shivpuri,[25] V. Simak,[7] P. Skubic,[68] P. Slattery,[64] D. Smirnov,[51] K.J. Smith,[63] G.R. Snow,[60] J. Snow,[67] S. Snyder,[66] S. Söldner-Rembold,[41] L. Sonnenschein,[18] K. Soustruznik,[6] J. Stark,[11] D.A. Stoyanova,[35] M. Strauss,[68] L. Suter,[41] P. Svoisky,[68] M. Titov,[15] V.V. Tokmenin,[32] Y.-T. Tsai,[64] D. Tsybychev,[65] B. Tuchming,[15] C. Tully,[62] L. Uvarov,[36] S. Uvarov,[36] S. Uzunyan,[47] R. Van Kooten,[49] W.M. van Leeuwen,[30] N. Varelas,[46] E.W. Varnes,[42] I.A. Vasilyev,[35] P. Verdier,[17] A.Y. Verkheev,[32] L.S. Vertogradov,[32] M. Verzocchi,[45] M. Vesterinen,[41] D. Vilanova,[15] P. Vokac,[7] H.D. Wahl,[44] M.H.L.S. Wang,[45] J. Warchol,[51] G. Watts,[75] M. Wayne,[51] J. Weichert,[21] L. Welty-Rieger,[48] A. White,[71] D. Wicke,[23] M.R.J. Williams,[39] G.W. Wilson,[53] M. Wobisch,[55] D.R. Wood,[56] T.R. Wyatt,[41] Y. Xie,[45]

R. Yamada,[45] S. Yang,[4] T. Yasuda,[45] Y.A. Yatsunenko,[32] W. Ye,[65] Z. Ye,[45] H. Yin,[45] K. Yip,[66] S.W. Youn,[45] J.M. Yu,[57] J. Zennamo,[63] T.G. Zhao,[41] B. Zhou,[57] J. Zhu,[57] M. Zielinski,[64] D. Zieminska,[49] and L. Zivkovic[14]

(The D0 Collaboration*)

[1]*LAFEX, Centro Brasileiro de Pesquisas Físicas, Rio de Janeiro, Brazil*
[2]*Universidade do Estado do Rio de Janeiro, Rio de Janeiro, Brazil*
[3]*Universidade Federal do ABC, Santo André, Brazil*
[4]*University of Science and Technology of China, Hefei, People's Republic of China*
[5]*Universidad de los Andes, Bogotá, Colombia*
[6]*Charles University, Faculty of Mathematics and Physics, Center for Particle Physics, Prague, Czech Republic*
[7]*Czech Technical University in Prague, Prague, Czech Republic*
[8]*Center for Particle Physics, Institute of Physics, Academy of Sciences of the Czech Republic, Prague, Czech Republic*
[9]*Universidad San Francisco de Quito, Quito, Ecuador*
[10]*LPC, Université Blaise Pascal, CNRS/IN2P3, Clermont, France*
[11]*LPSC, Université Joseph Fourier Grenoble 1, CNRS/IN2P3, Institut National Polytechnique de Grenoble, Grenoble, France*
[12]*CPPM, Aix-Marseille Université, CNRS/IN2P3, Marseille, France*
[13]*LAL, Université Paris-Sud, CNRS/IN2P3, Orsay, France*
[14]*LPNHE, Universités Paris VI and VII, CNRS/IN2P3, Paris, France*
[15]*CEA, Irfu, SPP, Saclay, France*
[16]*IPHC, Université de Strasbourg, CNRS/IN2P3, Strasbourg, France*
[17]*IPNL, Université Lyon 1, CNRS/IN2P3, Villeurbanne, France and Université de Lyon, Lyon, France*
[18]*III. Physikalisches Institut A, RWTH Aachen University, Aachen, Germany*
[19]*Physikalisches Institut, Universität Freiburg, Freiburg, Germany*
[20]*II. Physikalisches Institut, Georg-August-Universität Göttingen, Göttingen, Germany*
[21]*Institut für Physik, Universität Mainz, Mainz, Germany*
[22]*Ludwig-Maximilians-Universität München, München, Germany*
[23]*Fachbereich Physik, Bergische Universität Wuppertal, Wuppertal, Germany*
[24]*Panjab University, Chandigarh, India*
[25]*Delhi University, Delhi, India*
[26]*Tata Institute of Fundamental Research, Mumbai, India*
[27]*University College Dublin, Dublin, Ireland*
[28]*Korea Detector Laboratory, Korea University, Seoul, Korea*
[29]*CINVESTAV, Mexico City, Mexico*
[30]*Nikhef, Science Park, Amsterdam, the Netherlands*
[31]*Radboud University Nijmegen, Nijmegen, the Netherlands*
[32]*Joint Institute for Nuclear Research, Dubna, Russia*
[33]*Institute for Theoretical and Experimental Physics, Moscow, Russia*
[34]*Moscow State University, Moscow, Russia*
[35]*Institute for High Energy Physics, Protvino, Russia*
[36]*Petersburg Nuclear Physics Institute, St. Petersburg, Russia*
[37]*Institució Catalana de Recerca i Estudis Avançats (ICREA) and Institut de Física d'Altes Energies (IFAE), Barcelona, Spain*
[38]*Uppsala University, Uppsala, Sweden*
[39]*Lancaster University, Lancaster LA1 4YB, United Kingdom*
[40]*Imperial College London, London SW7 2AZ, United Kingdom*
[41]*The University of Manchester, Manchester M13 9PL, United Kingdom*
[42]*University of Arizona, Tucson, Arizona 85721, USA*
[43]*University of California Riverside, Riverside, California 92521, USA*
[44]*Florida State University, Tallahassee, Florida 32306, USA*
[45]*Fermi National Accelerator Laboratory, Batavia, Illinois 60510, USA*
[46]*University of Illinois at Chicago, Chicago, Illinois 60607, USA*
[47]*Northern Illinois University, DeKalb, Illinois 60115, USA*
[48]*Northwestern University, Evanston, Illinois 60208, USA*
[49]*Indiana University, Bloomington, Indiana 47405, USA*
[50]*Purdue University Calumet, Hammond, Indiana 46323, USA*
[51]*University of Notre Dame, Notre Dame, Indiana 46556, USA*
[52]*Iowa State University, Ames, Iowa 50011, USA*
[53]*University of Kansas, Lawrence, Kansas 66045, USA*
[54]*Kansas State University, Manhattan, Kansas 66506, USA*
[55]*Louisiana Tech University, Ruston, Louisiana 71272, USA*
[56]*Northeastern University, Boston, Massachusetts 02115, USA*
[57]*University of Michigan, Ann Arbor, Michigan 48109, USA*

[58]Michigan State University, East Lansing, Michigan 48824, USA
[59]University of Mississippi, University, Mississippi 38677, USA
[60]University of Nebraska, Lincoln, Nebraska 68588, USA
[61]Rutgers University, Piscataway, New Jersey 08855, USA
[62]Princeton University, Princeton, New Jersey 08544, USA
[63]State University of New York, Buffalo, New York 14260, USA
[64]University of Rochester, Rochester, New York 14627, USA
[65]State University of New York, Stony Brook, New York 11794, USA
[66]Brookhaven National Laboratory, Upton, New York 11973, USA
[67]Langston University, Langston, Oklahoma 73050, USA
[68]University of Oklahoma, Norman, Oklahoma 73019, USA
[69]Oklahoma State University, Stillwater, Oklahoma 74078, USA
[70]Brown University, Providence, Rhode Island 02912, USA
[71]University of Texas, Arlington, Texas 76019, USA
[72]Southern Methodist University, Dallas, Texas 75275, USA
[73]Rice University, Houston, Texas 77005, USA
[74]University of Virginia, Charlottesville, Virginia 22904, USA
[75]University of Washington, Seattle, Washington 98195, USA

(Dated: January 10, 2013)

We measure the ratio of cross sections, $\sigma(p\bar{p} \to Z + b \text{ jet})/\sigma(p\bar{p} \to Z + \text{jet})$, for associated production of a Z boson with at least one jet. The ratio is also measured as a function of the jet transverse momentum, jet pseudorapidity, Z boson transverse momentum, and the azimuthal angle between the Z boson and the closest jet for events with at least one b jet. These measurements use data collected by the D0 experiment in Run II of Fermilab's Tevatron $p\overline{p}$ Collider at a center-of-mass energy of 1.96 TeV, and correspond to an integrated luminosity of 9.7 fb^{-1}. The results are compared to predictions from next-to-leading order calculations and various Monte Carlo event generators.

PACS numbers: 12.38.Qk, 13.85.Qk, 14.65.Fy, 14.70.Hp

I. INTRODUCTION

Studies of Z boson production in association with jets from b quarks, or b jets, provide important tests of the predictions of perturbative quantum chromodynamics (pQCD) [1]. A good theoretical description of this process is essential since it forms a major background for a variety of physics processes, including the standard model (SM) Higgs boson production in association with a Z boson, $ZH(H \to b\bar{b})$ [2], and searches for supersymmetric partners of the b quark [3]. Furthermore, $Z+b$ jet production can serve as a reference process for a non-SM Higgs boson (h) produced in association with a b quark. Two different approaches are currently available to calculate Z or h boson production in association with a b quark at next-to-leading order (NLO) [1, 4]. They yield consistent results within theoretical uncertainties [5].

The ratio of $Z + b$ jet to $Z +$ jet production cross sections, for events with one or more jets, has been previously measured by the CDF [6, 7] and D0 [8, 9] collaborations using a fraction of the Run II data. The results obtained by the two experiments agree, within experimental uncertainties, and with the theoretical predictions.

The current measurement is based on the complete Run II data sample collected by the D0 experiment [10] at Fermilab's Tevatron $p\overline{p}$ collider running with a center-of-mass energy of $\sqrt{s} = 1.96$ TeV, and corresponds to an integrated luminosity of 9.7 fb^{-1}. The enlarged data sample enables the measurement of the cross section ratio, $\sigma(Z + b \text{ jet})/\sigma(Z + \text{jet})$, to be performed differentially as a function of various kinematic variables. The Z bosons are required to decay to pairs of leptons, $\mu\mu$ or ee, and pass at least one of the single electron or muon triggers. The $Z +$ jet sample requires the presence of at least one jet in the event, while the $Z + b$ jet sample requires at least one b-jet candidate, selected using a b-tagging algorithm [11]. For our off-line event selection, the triggers have an efficiency of approximately 100% for $Z \to ee$ and more than 78% for $Z \to \mu\mu$ decays depending on the transverse momentum of the muon. The measurement of the ratio of cross sections benefits from nearly complete cancellation of several systematic uncertainties such as those associated with the identification of leptons, jets, measurement of the luminosity, etc., and therefore allows for a more precise comparison of data with various theoretical predictions.

This analysis relies on all components of the D0 detector: tracking, calorimetry, muon reconstruction and

*with visitors from [a]Augustana College, Sioux Falls, SD, USA, [b]The University of Liverpool, Liverpool, UK, [c]UPIITA-IPN, Mexico City, Mexico, [d]DESY, Hamburg, Germany, [e]SLAC, Menlo Park, CA, USA, [f]University College London, London, UK, [g]Centro de Investigacion en Computacion - IPN, Mexico City, Mexico, [h]ECFM, Universidad Autonoma de Sinaloa, Culiacán, Mexico and [i]Universidade Estadual Paulista, São Paulo, Brazil.

the ability to identify secondary vertices. The D0 detector [10] consists of a central tracking system, comprising a silicon microstrip tracker (SMT) and a central fiber tracker, both located within a 2 T solenoidal magnet; a liquid-argon sampling calorimeter divided into a central calorimeter (CC) and two endcap calorimeters (EC) with four electromagnetic (EM) and four to five hadronic sections in depth. The outermost part of the D0 detector, the muon system is composed of three layers of drift tubes and scintillating trigger counters, one layer before and two layers after a 1.8 T toroidal magnet. A precise reconstruction of the primary $p\overline{p}$ interaction vertex [12] and secondary vertices is facilitated by the SMT. It also enables an accurate determination of the impact parameter, defined as a distance of closest approach of a track to the interaction vertex. The impact parameter measurements of tracks, along with the secondary vertices, are important inputs to the b-tagging algorithm.

II. EVENT SELECTION

An event is selected if it contains a $p\overline{p}$ interaction vertex, built from at least three tracks, located within 60 cm of the center of the D0 detector along the beam axis. The selected events must also contain a Z boson candidate with a dilepton invariant mass $70 < M_{\ell\ell} < 110$ GeV ($\ell = e, \mu$).

Dielectron (ee) events are required to have two electrons of transverse momentum $p_T > 15$ GeV identified through EM showers in the calorimeter. The showers must have more than 90% of their energy deposited in the EM calorimeter, be isolated from other energy depositions, and have a transverse and longitudinal profile consistent with that expected for an electron. At least one electron must be identified in the CC, within a pseudorapidity [13] region $|\eta| < 1.1$, and a second electron either in the CC or the EC, $1.5 < |\eta| < 2.5$. Electron candidates in the CC region are also required to match central tracks or have a pattern of hits consistent with the passage of an electron through the central tracker. There is no requirement on the charge of the selected electrons.

Dimuon ($\mu\mu$) events are required to have two oppositely charged muons detected in the muon spectrometer that are matched to central tracks with $p_T > 10$ GeV and $|\eta| < 2$. At least one muon is required to have $p_T > 15$ GeV. These muons must pass a combined tracking and calorimeter isolation requirement. Muons originating from cosmic rays are rejected by applying timing criteria using the hits in the scintillator layers and by limiting the measured displacement of the muon track with respect to the $p\overline{p}$ interaction vertex.

A total of 1,249,911 Z boson candidate events are retained in the combined ee and $\mu\mu$ channels with the above criteria. The Z + jet sample is then selected by requiring at least one jet in the event with $p_T^{\rm jet} > 20$ GeV and $|\eta^{\rm jet}| < 2.5$. Jets are reconstructed from energy deposits in the calorimeter using an iterative midpoint cone algorithm [14] with a cone of radius $\Delta R = \sqrt{(\Delta\varphi)^2 + (\Delta y)^2} = 0.5$ where φ is the azimuthal angle and y is the rapidity. Jet energy is corrected for detector response, the presence of noise, multiple $p\bar{p}$ interactions, and energy deposited outside of the jet cone used for reconstruction [15].

To suppress background from top quark production, events are rejected if the missing transverse energy is larger than 60 GeV, reducing the $t\bar{t}$ contamination by a factor of two. These selection criteria retain an inclusive sample of 176,498 Z + jet event candidates in the combined ee and $\mu\mu$ channel.

III. MODELING OF EVENTS

Processes such as diboson (WW, WZ, ZZ) production can contribute to the background when two leptons are reconstructed in the final state. Inclusive diboson production is simulated with the PYTHIA [16] Monte Carlo (MC) event generator. The Z + jet, including heavy flavor jets, and $t\bar{t}$ events are modeled by ALPGEN [17], which generates hard sub-processes including higher order QCD tree level matrix elements, interfaced with PYTHIA for parton showering and hadronization. The CTEQ6L1 [18] parton distribution functions (PDFs) are used in all simulations. The cross sections of the simulated samples are then scaled to the corresponding higher order theoretical calculations. For the diboson and Z + jet processes, including the $Z + b\bar{b}$ signal process and $Z + c\bar{c}$ production, next-to-leading order (NLO) cross section predictions are taken from MCFM [19]. The $t\bar{t}$ cross section is determined from approximate next-to-NLO calculations [20]. To improve the modeling of the p_T distribution of the Z boson, simulated Z + jet events are also reweighted to be consistent with the measured p_T spectrum of Z bosons observed in data [21].

These generated samples are processed through a detailed detector simulation based on GEANT [22]. To model the effects of detector noise and pile-up events, collider data from random beam crossings are superimposed on simulated events. These events are then reconstructed using the same algorithms as used for data. Scale factors, determined from data using independent samples, are applied to account for differences in reconstruction efficiency between data and simulation. The energies of simulated jets are corrected, based on their flavor, to reproduce the resolution and energy scale observed in data [15]. In the following, light-quark flavor (u, d, s) and gluon jets are referred to as "light jets" or "LF".

The background contribution from multijet instrumental background events, in which jets are misidentified as leptons, is evaluated from data. This is performed using a multijet-enriched sample of events that pass all selection criteria except for some of the lepton quality requirements. In the case of electrons, the multijet sam-

ple is obtained by inverting the shower shape requirement and relaxing other electron identification criteria, while for the muon channel, the multijet sample consists of events with muon candidates that fail the isolation requirements. The normalization of the multijet background is determined from a simultaneous fit to the dilepton invariant mass distributions in the different jet multiplicity bins.

Figure 1 shows the leading jet p_T distributions, where leading jet refers to the jet with the highest p_T, compared to the expectations from various processes. The dominant contribution comes from Z+light jet production. The background fraction in the ee channel is about 9.6%, and is dominated by multijet production. The muon channel has a higher purity with a background fraction of less than 1.3%.

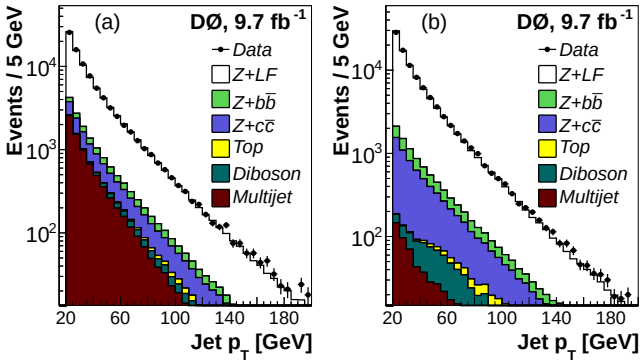

FIG. 1: (color online) The leading jet p_T in the (a) $Z \to ee$ and (b) $Z \to \mu\mu$ channels for data and background in events with a Z boson candidate and at least one jet before b tagging is applied.

IV. b JET IDENTIFICATION

This analysis employs a two-step procedure to determine the b quark content of jets in the selected events. First, a b-tagging algorithm is applied to jets to select a sample of Z + jet events that is enriched in heavy flavor jets. After b tagging, the relative light, charm, and b quark content is extracted by fitting templates built from a dedicated discriminant that provides an optimized separation between the three components.

Jets considered for b-tagging are subject to a preselection requirement, called taggability, to decouple the intrinsic performance of the b jet tagging algorithm from effects related to track reconstruction efficiency. For this purpose, the jet is required to have at least two associated tracks with $p_T > 0.5$ GeV, the leading track must have $p_T > 1$ GeV, and each track must have at least one SMT hit. This requirement has a typical efficiency of 90% per b jet.

The b-tagging algorithm is based on a multivariate analysis (MVA) technique [23]. This algorithm, known as the MVA$_{bl}$ since it discriminates b-like jets from light-flavor-like jets, utilizes the relatively long lifetime of the b hadrons when compared to their lighter counterparts [11]. Events with at least one jet tagged by this algorithm are considered.

The MVA$_{bl}$ discriminant combines various properties of the jet and associated tracks to create a continuous output that tends towards unity for b jets and zero for light jets. The input variables include the number of reconstructed secondary vertices in the jet, the invariant mass of the charged particles associated with the secondary vertex ($M_{\rm SV}$) with the largest decay length significance (defined as the transverse decay length divided by its uncertainty), the number of tracks in the reconstructed secondary vertex, the decay length significance of the secondary vertex, the weighted sum of the transverse impact parameter significance of tracks, and the Jet Lifetime Probability (JLIP), which is the probability that tracks associated with the jet originate from the $p\overline{p}$ interaction vertex. Events are retained for further analysis if they contain at least one jet with an MVA$_{bl}$ output greater than 0.1 and a valid secondary vertex with $M_{\rm SV} > 0$ GeV; the latter assumes that a secondary vertex can be associated with the jet. After these requirements, 4,114 Z + jet events are selected with at least one b-tagged jet, where only the highest p_T tagged jet is examined in the analysis. The efficiency for tagging b, c, and light jets are approximately 40%, 10%, and 0.4%, respectively. The resulting background contamination from diboson, multijet, and top production after b-tagging, for the electron and muon channels are 10.4% and 4.8%, respectively.

V. EXTRACTION OF b JET FRACTION

To determine the fraction of events with b, c and light jets, a dedicated discriminant, $D_{\rm MJL}$, is employed [9]. It is a combination of the two most discriminating variables mentioned above, $M_{\rm SV}$ and JLIP: $D_{\rm MJL} = 0.5 \times (M_{\rm SV}/5\ {\rm GeV} - \ln({\rm JLIP})/20)$. The coefficients in this equation are chosen empirically to ensure that the bulk of the $D_{\rm MJL}$ values fall between zero and one. Figure 2(a) shows the $D_{\rm MJL}$ distributions (templates) obtained from simulations of all three considered jet flavors that pass the b-tagging requirement. Also shown in Fig. 2(a) is the corresponding distribution for a light jet enriched data sample, known as "negatively tagged jets", which are used to assess the systematic uncertainty of the light jet template shape. These jets have negative values for the decay length significance and/or impact parameter, which are caused by the detector resolution effects [11]. We estimate the b jet contamination in the negatively tagged data using a maximum likelihood fit and subtract its contribution. A small difference in the shape of the light jet templates, as measured in the negatively tagged data and simulated light jet samples, is taken as a systematic uncertainty.

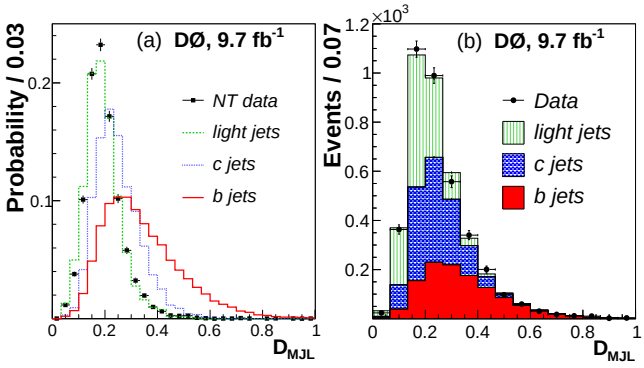

FIG. 2: (color online) (a) The probability densities of the $D_{\rm MJL}$ discriminant for b, c, and light jets passing the b tagging requirements, normalized to unity. These templates are taken from MC simulations. Also shown is the distribution for the negatively tagged (NT) jets in data. (b) The $D_{\rm MJL}$ discriminant distribution of events in the combined sample. The distributions of the b, c, and light jets are normalized by the fractions found from the fit.

To measure the fraction of events with different jet flavors in the selected sample, we perform a binned maximum likelihood fit to the $D_{\rm MJL}$ distribution in data using the b, c, and light flavor jet templates. Before the fit, all background contributions estimated after the MVA$_{bl}$ requirement, i.e., multijet, diboson and $t\bar{t}$ production, are subtracted from the data leaving 1,854 and 1,946 $Z+$jet events in the ee and $\mu\mu$ channels, respectively. Next, we measure the jet-flavor fractions in the dielectron and dimuon samples separately, yielding the b jet flavor fractions of 0.284 ± 0.028 (stat.) and 0.333 ± 0.026 (stat.), respectively. Since these measurements are in agreement within their statistical uncertainties, we combine the two samples to increase the statistical power of the fit for individual jet flavors. The measured fraction of b jets in the combined sample is 0.300 ± 0.019 (stat.), the combined $D_{\rm MJL}$ distribution of the b-tagged data and the fitted templates for the b, c, and light jets are shown in Fig. 2(b).

VI. MEASUREMENT OF THE CROSS SECTION RATIO

The measured fraction of b jets in the selected sample of $Z+$jet event candidates can now be combined with the corresponding acceptances for events, estimated using simulations, to determine the ratio of cross sections using

$$\frac{\sigma(Z+b\text{ jet})}{\sigma(Z+\text{jet})} = \frac{N\, f_b}{N_{\rm incl}\,\epsilon^b_{tag}} \times \frac{\mathcal{A}_{\rm incl}}{\mathcal{A}_b}, \qquad (1)$$

where $N_{\rm incl}$ is the total number of Z+jet events before the tagging requirements, N is the number of $Z+$jet events used in the $D_{\rm MJL}$ fit, f_b is the extracted b jet fraction, and ϵ^b_{tag} is the overall selection efficiency of $D_{\rm MJL}$ for b jets which combines the efficiencies for taggability, MVA$_{bl}$ discriminant and $D_{\rm MJL}$ selection. Both $N_{\rm incl}$ and N correspond to the number of events that remain after the contributions from non-$Z+$jet processes have been subtracted from the data.

The detector acceptances for the inclusive jet sample ($\mathcal{A}_{\rm incl}$) and b jets ($\mathcal{A}_b$) are determined from simulations in the kinematic region that satisfies the p_T and η requirements for leptons and jets. The resulting ratio of the two acceptances is measured to be $\mathcal{A}_{\rm incl}/\mathcal{A}_b = 1.118 \pm 0.002$ (stat.). In this ratio, the effect of migration of events near the kinematic threshold, or between neighboring kinematic bins, due to the finite detector resolution is found to be negligibly small.

Using Eq. (1), the result for the ratio of the $Z+b$ jet cross section to the inclusive $Z+$jet cross section in the combined $\mu\mu$ and ee channel is 0.0202 ± 0.0014 (stat.). In addition, the ratio $\sigma(Z+b\text{ jet})/\sigma(Z+\text{jet})$ of differential cross sections as a function of $p_T^{\rm jet}$, $\eta^{\rm jet}$, p_T^Z, and the azimuthal angle, $\Delta\varphi_{Z,\rm jet}$, between the Z boson and the closest jet in the event, is measured. The data are split into five bins for each variable such that the sample sizes allow for a stable fit with the $D_{\rm MJL}$ templates. The templates, in turn, are constructed individually for every bin in the distribution of each examined variable. The selected bin sizes along with the corresponding statistics of data events used in the fit are listed in Table I. In each case, all the quantities that enter into Eq. (1) are remeasured separately. A summary of the differential cross section ratio measurements can also be found in Table I.

VII. SYSTEMATIC UNCERTAINTIES

Several systematic uncertainties cancel when the ratio $\sigma(Z+b\text{ jet})/\sigma(Z+\text{jet})$ is measured. These include uncertainties on the luminosity measurement, trigger, lepton, and the jet identification efficiencies. The remaining uncertainties are estimated separately for the integrated result and in each bin of the differential distributions. For the integrated result, the largest systematic uncertainty of 7.6% is due to the b jet energy calibration; it comprises the uncertainties on the jet energy resolution and the jet energy scale. The next largest systematic uncertainty of 3.9% comes from the shape of the $D_{\rm MJL}$ templates used in the fit. The shape of the templates may be affected by the choice of the b quark fragmentation function [25], the background estimation, the difference in the shape of the light jet MC and negatively tagged data templates, the composition of the charm states used to determine the charm template shape [9], and the uncertainty from the fit itself. These effects are evaluated by varying the central values by the corresponding uncertainties, one at a time, and repeating the entire analysis chain. The other sources of uncertainty are due to the b jet identification efficiency (1.8%) and the choice of the MC event gen-

TABLE I: Results for the ratio $\sigma(Z+b\text{ jet})/\sigma(Z+\text{jet})$ in bins of p_T^{jet}, p_T^Z, η^{jet}, and $\Delta\varphi_{Z,\text{jet}}$. Bin centers, shown in parentheses, are chosen using the prescription found in Ref. [24].

p_T^{jet} [GeV]	N	$\frac{\sigma(Z+b\text{ jet})}{\sigma(Z+\text{jet})}$	Statistical Uncertainty	Systematic Uncertainty
$20-30$ (25)	1317	0.0175	0.0010	0.0022
$30-40$ (35)	858	0.0192	0.0012	0.0019
$40-55$ (47)	712	0.0210	0.0016	0.0015
$55-70$ (62)	369	0.0231	0.0025	0.0021
$70-200$ (102)	535	0.0226	0.0033	0.0022
p_T^Z [GeV]				
$0-20$ (12)	502	0.0283	0.0029	0.0050
$20-40$ (32)	1326	0.0112	0.0007	0.0010
$40-60$ (50)	998	0.0200	0.0011	0.0012
$60-80$ (68)	512	0.0236	0.0018	0.0016
$80-200$ (100)	453	0.0334	0.0034	0.0025
η^{jet}				
$0-0.25$ (0.13)	614	0.0131	0.0012	0.0010
$0.25-0.5$ (0.38)	639	0.0164	0.0014	0.0012
$0.5-1.0$ (0.75)	1180	0.0209	0.0010	0.0018
$1.0-1.5$ (1.25)	888	0.0213	0.0014	0.0027
$1.5-2.5$ (2.00)	477	0.0152	0.0017	0.0027
$\Delta\varphi_{Z,\text{jet}}$ [rad]				
$0-2.5$ (1.62)	833	0.0292	0.0019	0.0040
$2.5-2.75$ (2.63)	514	0.0212	0.0024	0.0023
$2.75-2.9$ (2.83)	596	0.0215	0.0015	0.0020
$2.9-3.05$ (2.98)	961	0.0151	0.0009	0.0012
$3.05-3.2$ (3.13)	895	0.0131	0.0010	0.0009

erator, ALPGEN or PYTHIA, for the detector acceptance evaluations ($< 0.1\%$). For the integrated ratio measurement, these uncertainties, when summed in quadrature, result in a total systematic uncertainty of 8.7%. The corresponding total systematic uncertainties for the ratios of differential cross sections are listed in Table I, while Table II lists them separately for each variable and bin. Finally, for the integrated $\sigma(Z+b\text{ jet})/\sigma(Z+\text{jet})$ ratio we obtain a value of $0.0202\pm0.0014\,(\text{stat.})\pm0.0018\,(\text{syst.})$ which is in agreement with the previous D0 result of 0.0193 ± 0.0027 [9].

VIII. COMPARISON TO PREDICTIONS

The measurements are compared to predictions from an NLO pQCD calculation and two leading order MC event generators, SHERPA [26] and ALPGEN. The NLO predictions are based on MCFM [1], version 5.6, with the MSTW2008 PDFs [27] and the renormalization and factorization scales set at $Q_R^2 = Q_F^2 = M_Z^2 + \sum (p_T^{\text{jet}})^2$. Here, M_Z is the Z boson mass and p_T^{jet} is the transverse momentum of the jet(s). The measurement above is in agreement with the NLO pQCD prediction of $0.0206^{+0.0022}_{-0.0013}$ [1], with corrections to account for non-perturbative effects estimated using ALPGEN+PYTHIA. Uncertainties on the theoretical predictions are evaluated by simultaneously changing the renormalization and factorization scales up or down by a factor of two.

Compared to an NLO calculation, SHERPA uses the CKKW matching scheme between the leading-order matrix element partons and the parton-shower jets following the prescription given in Ref. [28]. This effectively allows for a consistent combination of the matrix element and parton shower.

ALPGEN also generates multi-parton final states using tree-level matrix elements. When interfaced with PYTHIA, it employs an MLM scheme [29] to match matrix element partons with those after showering in PYTHIA, resulting in an improvement over leading-logarithmic accuracy.

The ratio of differential cross sections as a function of p_T^{jet}, p_T^Z, η^{jet}, and $\Delta\varphi_{Z,\text{jet}}$ are compared to predictions from MCFM, ALPGEN, and SHERPA in Fig. 3. None of the predictions can fully describe all the examined variables, except for the p_T^{jet}. Based on a χ^2 test we find that the dependence on the p_T^Z and $\Delta\varphi_{Z,\text{jet}}$ correlation are best described by ALPGEN and SHERPA, respectively. Overall the integrated result is best described by MCFM NLO predictions.

IX. CONCLUSIONS

We have measured the ratio of integrated cross sections, $\sigma(p\bar{p} \to Z + b\text{ jet})/\sigma(p\bar{p} \to Z + \text{jet})$, as well as the ratio of the differential cross sections in bins of p_T^{jet}, p_T^Z, η^{jet}, and $\Delta\varphi_{Z,\text{jet}}$, for events with $Z \to \ell\ell (\ell = e, \mu)$ and at least one b jet in the final state. Measurements are based on the full data sample collected by the D0 experiment in Run II of the Tevatron, corresponding to an integrated luminosity of 9.7 fb^{-1} at a center-of-mass energy of 1.96 TeV. For jets with $p_T^{\text{jet}} > 20$ GeV and pseudorapidity $|\eta^{\text{jet}}| < 2.5$, the measured integrated ratio of $0.0202\pm0.0014\,(\text{stat.})\pm0.0018\,(\text{syst.})$ is in agreement with NLO pQCD predictions. Results for the ratio of differential cross sections are also compared to predictions from two Monte Carlo event generators. None of the predictions provide a consistent description of all the examined variables.

We thank the authors of Refs. [1, 5, 26] for valuable discussions, and the staffs at Fermilab, and collaborating institutions, and acknowledge support from the DOE and NSF (USA); CEA and CNRS/IN2P3 (France); MON, NRC KI and RFBR (Russia); CNPq, FAPERJ, FAPESP and FUNDUNESP (Brazil); DAE and DST (India); Colciencias (Colombia); CONACyT (Mexico); NRF (Korea); FOM (The Netherlands); STFC and the Royal Society (United Kingdom); MSMT and GACR (Czech Republic); BMBF and DFG (Germany); SFI (Ireland); The Swedish Research Council (Sweden); and CAS and CNSF (China).

TABLE II: Systematic uncertainties for the ratio of differential cross sections.

Source of Systematic Uncertainty	Uncertainty [%]				
$p_T^{\rm jet}$ [GeV]	$20-30$	$30-40$	$40-55$	$55-70$	$70-200$
Jet Energy Scale, Resolution	10.7	7.4	4.3	4.9	2.6
Template Shape	5.7	4.9	5.1	6.3	6.8
b tagging	1.2	1.4	1.9	2.5	2.6
Acceptance	3.3	3.4	0.4	3.2	5.9
p_T^Z [GeV]	$0-20$	$20-40$	$40-60$	$60-80$	$80-200$
Jet Energy Scale, Resolution	16.4	5.7	2.0	0.8	1.5
Template Shape	6.1	4.8	5.1	6.2	6.4
b tagging	1.6	1.7	1.8	1.9	2.1
Acceptance	1.1	4.8	0.2	1.8	3.2
$\eta^{\rm jet}$	$0-0.25$	$0.25-0.5$	$0.5-1.0$	$1.0-1.5$	$1.5-2.5$
Jet Energy Scale, Resolution	4.3	4.0	5.8	9.6	12.9
Template Shape	5.9	5.5	5.3	5.9	6.9
b tagging	1.3	1.3	1.4	1.5	5.7
Acceptance	1.5	2.2	2.7	5.1	8.6
$\Delta\varphi_{Z,\rm jet}$ [rad]	$0-2.5$	$2.5-2.75$	$2.75-2.9$	$2.9-3.05$	$3.05-3.2$
Jet Energy Scale, Resolution	11.5	8.8	6.6	5.3	3.8
Template Shape	6.6	5.6	5.5	4.8	4.9
b tagging	1.7	1.8	2.0	2.0	1.9
Acceptance	3.1	2.5	2.2	1.9	1.8

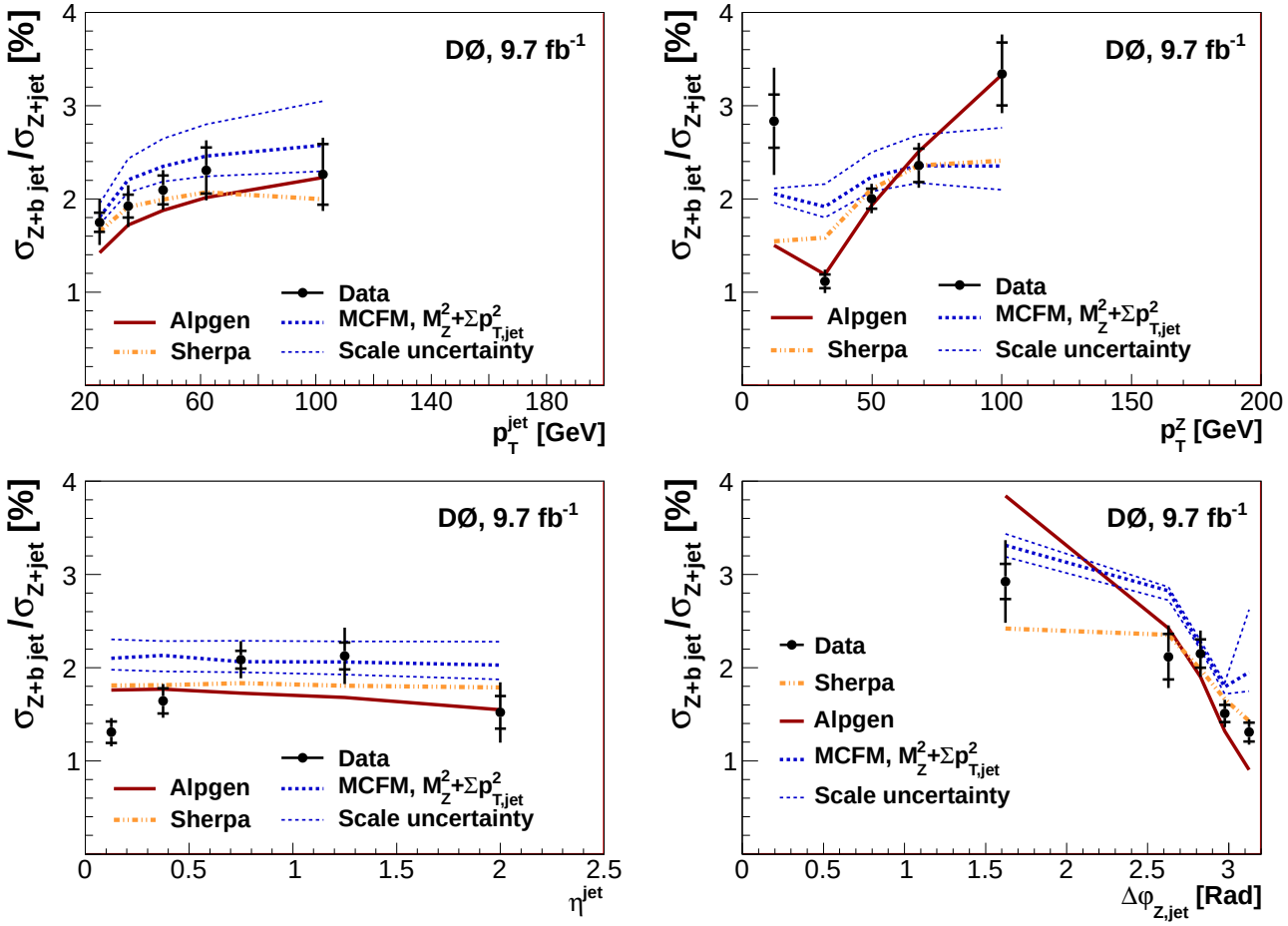

FIG. 3: (color online) Ratios of the differential cross sections. The uncertainties on the data include statistical (inner error bar) and full uncertainties (entire error bar). The data are compared to the prediction from ALPGEN, SHERPA, and the MCFM NLO calculation, where the band represents the variation of the renormalization and factorization scales up and down by a factor of two. Bin centers are chosen using the prescription found in Ref. [24].

[1] J. M. Campbell, R. K. Ellis, F. Maltoni, and S. Willenbrock, Phys. Rev. D **69**, 074021 (2004).

[2] V. M. Abazov *et al.* (D0 Collaboration), Phys. Rev. Lett. **109**, 121803 (2012); T. Aaltonen *et al.* (CDF Collaboration), Phys. Rev. Lett. **109**, 111803 (2012).

[3] V. M. Abazov *et al.* (D0 Collaboration), Phys. Lett. B **693**, 95 (2010); T. Aaltonen *et al.* (CDF Collaboration), Phys. Rev. Lett. **105**, 081802 (2010).

[4] F. F. Cordero, L. Reina, and D. Wackeroth, Phys. Rev. D **78**, 074014 (2008).

[5] S. Dawson, C. B. Jackson, L. Reina, and D. Wackeroth, Modern Phys. Lett. A **21**, 89 (2006).

[6] T. Aaltonen *et al.* (CDF Collaboration), Phys. Rev. D **79**, 052008 (2009).

[7] A. Abulencia *et al.* (CDF Collaboration), Phys. Rev. D **74**, 032008 (2006).

[8] V. M. Abazov *et al.* (D0 Collaboration), Phys. Rev. Lett. **94**, 161801 (2005).

[9] V. M. Abazov *et al.* (D0 Collaboration), Phys. Rev. D **83**, 031105 (2011).

[10] V.M. Abazov *et al.* (D0 Collaboration), Nucl. Instrum. Methods Phys. Res. A **565**, 463 (2006); M. Abolins *et al.*, Nucl. Instrum. Methods Phys. Res. A **584**, 75 (2008); R. Angstadt *et al.*, Nucl. Instrum. Methods Phys. Res. A **622**, 298 (2010).

[11] V. M. Abazov *et al.* (D0 Collaboration), Nucl. Instrum. Methods Phys. Res. Sect. A **620**, 490 (2010).

[12] The primary $p\overline{p}$ interaction vertex is that found to be the most likely collision point, among possibly several collisions within a specific beam crossing, from which our selected objects emanate. The algorithm for defining it can be found in [11].

[13] Pseudorapidity is defined as $\eta = -\ln[\tan(\theta/2)]$, with the polar angle θ measured relative to the proton beam direction.

[14] G. C. Blazey *et al.*, arXiv:hep-ex/0005012.

[15] V. M. Abazov *et al.* (D0 Collaboration), Phys. Rev. D **85**, 052006 (2012).

[16] T. Sjöstrand, S. Mrenna, and P. Skands, J. High Energy Phys. **05**, 026 (2006). Version 6.409 with Tune A was used.

[17] M. L. Mangano *et al.*, J. High Energy Phys. **07**, 001 (2003). Version 2.11 was used.

[18] J. Pumplin *et al.*, J. High Energy Phys. **07**, 012 (2002).

[19] J. M. Campbell and R. K. Ellis, Phys. Rev. D **60**, 113006 (1999); ibid. **62**, 114012 (2000); ibid. **65**, 113007 (2002).

[20] U. Langenfeld, S. Moch, and P. Uwer, Phys. Rev. D **80**, 054009 (2009).

[21] V. M. Abazov *et al.* (D0 Collaboration), Phys. Rev. Lett. **100**, 102002 (2008).

[22] R. Brun and F. Carminati, CERN Program Library Long Writeup W5013 (1993).

[23] A. Hoecker *et al.*, TMVA: Toolkit for Multivariate Data Analysis. PoS, ACAT:040, 2007.

[24] G.D. Lafferty, and T.R. Wyatt, Nucl. Instrum. Methods Phys. Res. Sect. A **355**, 541 (1995).

[25] V. M. Abazov *et al.* (D0 Collaboration), Phys. Rev. D **84**, 032004 (2011).

[26] T. Gleisberg *et al.*, J. High Energy Phys. **02**, 007 (2009).

[27] A. D. Martin, W. J. Stirling, R. S. Thorne, and G. Watt, Eur. Phys. J. C **63**, 189 (2009).

[28] S. Catani *et al.*, J. High Energy Phys. **11**, 063 (2001).

[29] F. Caravaglios *et al.*, Nucl. Phys. B **539**, 215 (1999).